Supporting Information

Wang et al. 10.1073/pnas.1214088109

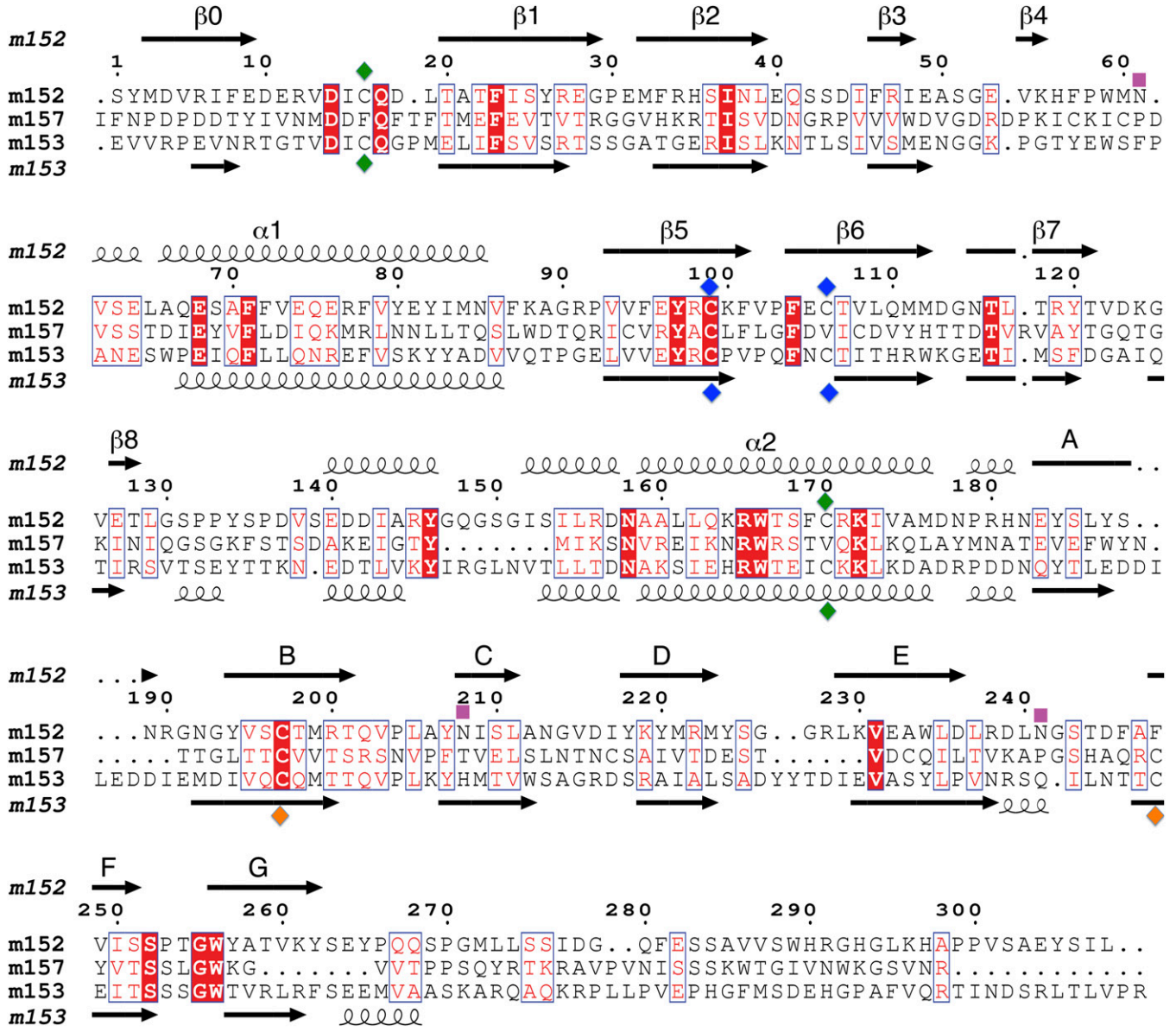

Fig. S1. Structure-based alignment of m152, m153, and m157. Amino acid sequences (extracellular domain) of the indicated proteins were aligned with ClustalW as a first guide, and alignments were further arranged based on the secondary structures of m152 and m153 by ESpript 2.2 (secondary structures of m152 and m153 are indicated). Cysteine residues involved in the disulfide bond linkages are indicated by green or blue diamonds (m152) and by green, blue, or orange diamonds (m153). Predicted N-linked glycosylation sites of m152 are indicated by pink squares.

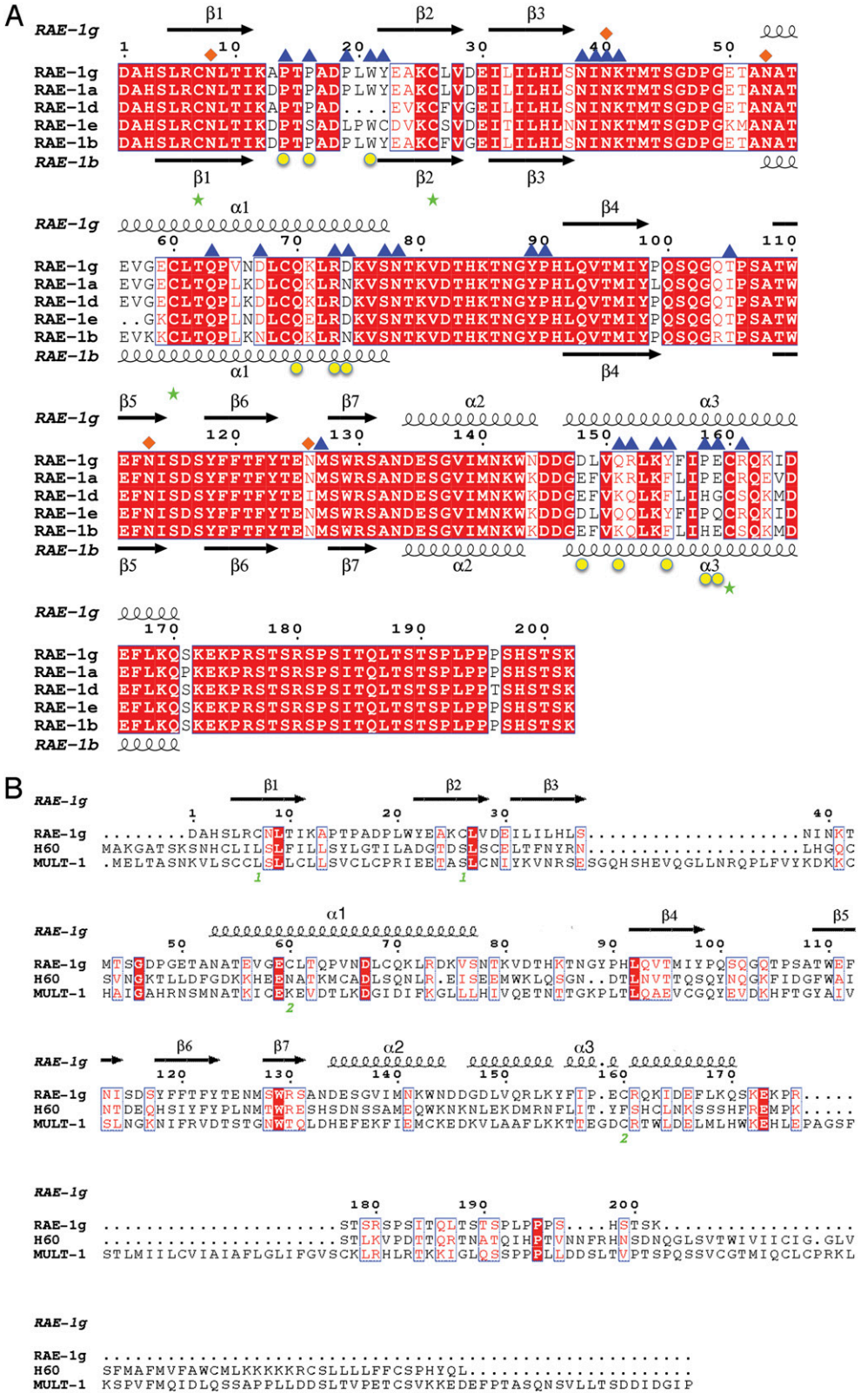

Fig. S2. Structure-based sequence alignment of RAE1 isoforms (*A*) and RAE1γ with H60 and murine UL16-binding protein-like transcript 1 (MULT1) (*B*). (*A*) The extracellular domains of RAE1 isoforms were first aligned with Clustal W, followed by secondary structural alignment with Espript 2.2. RAE1γ residues that contact or form hydrogen bonds to m152 are indicated by blue triangles. RAE1β residues that contact mNKG2D are indicated by yellow circles. Orange diamonds indicate potential *N*-asparaginyl-glycosylation sites. Green stars indicate cysteine residues involved in disulfide bonds. Indicated contact sites are from the first heterodimer in the asymmetric unit. (*B*) Sequence alignment of RAE1γ, H60, and MULT1.

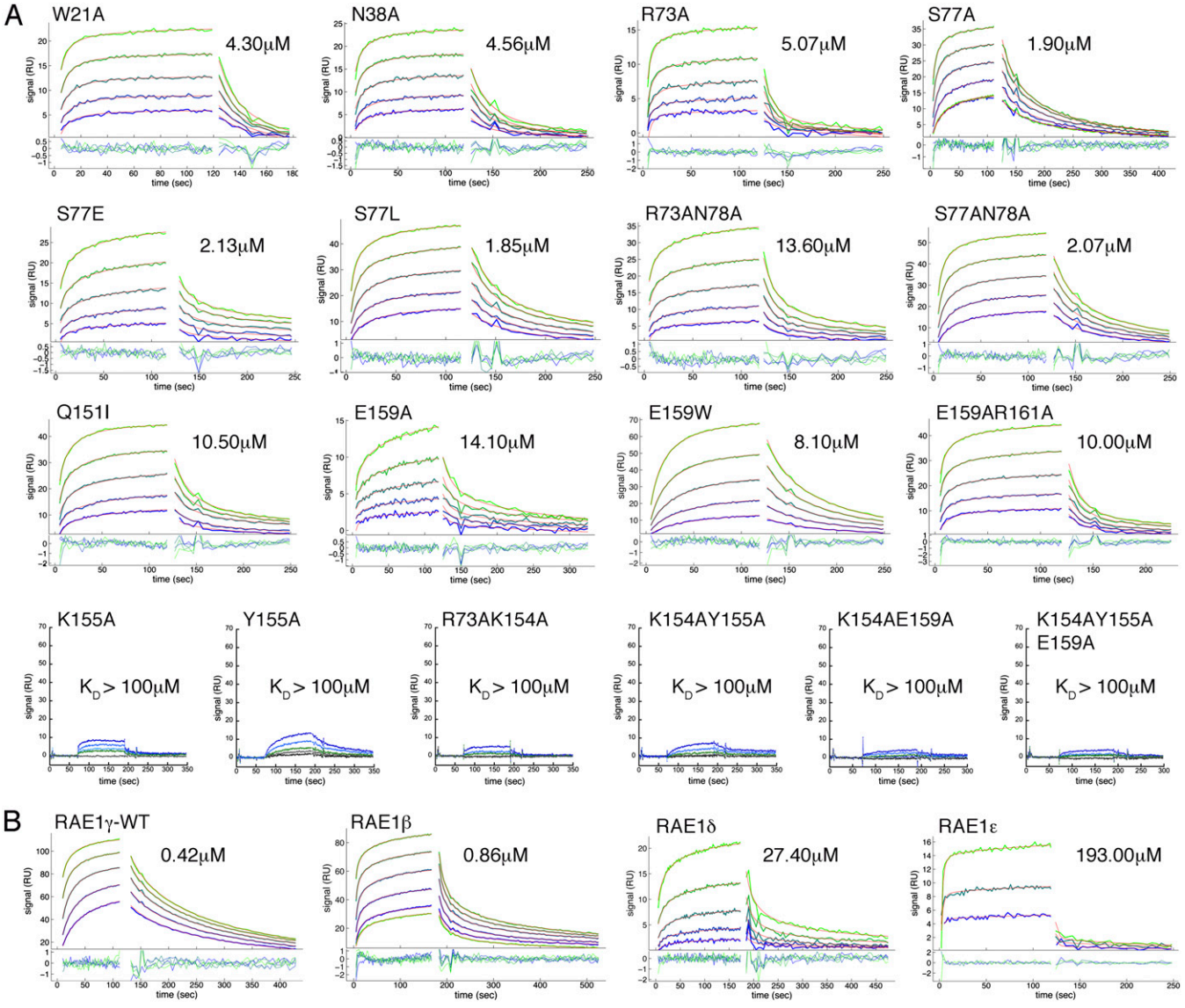

C

	K_D (M)	k_{off} (s^{-1})	r.m.s.d.		K_D (M)	k_{off} (s^{-1})	r.m.s.d.
RAE1γWT	4.15e-07	9.42e-03	0.36	S77A/N78A	2.07e-06	2.91e-02	0.37
W21A	4.30e-06	6.82e-02	0.26	Q151I	1.05e-05	4.62e-02	0.40
N38A	4.56e-06	2.72e-02	0.32	E159A	1.41e-05	3.36e-03	0.26
R73A	5.07e-06	8.40e-02	0.32	E159W	8.10e-06	2.02e-02	0.35
S77A	1.90e-06	2.90e-02	0.34	E159A/R161A	1.00e-05	5.33e-02	0.44
S77E	2.13e-06	4.05e-02	0.30	RAE1β	8.63e-07	7.43e-02	0.40
S77L	1.85e-06	3.46e-02	0.37	RAE1δ	2.74e-05	3.56e-02	0.39
R73A/N78A	1.35e-05	1.06e-02	0.30	RAE1ε	1.93e-04	5.13e-01	0.37

Fig. S3. Surface plasmon resonance (SPR) binding of RAE1 to the m152 surface. (*A*) Binding traces of indicated RAE1 mutants. (*B*) Binding isotherms of different RAE1 isoforms. m152 was coupled to CM5 biosensor chips, and RAE1γ, β, δ, or ε or RAE1γ mutants were sequentially injected over the surface. The zero time point corresponds to the start of the injection. Background binding to a mock-coupled surface was subtracted. Calculated K_d values were determined by EVILFIT or BIAevaluation 3.0 for poor binding. (For EVILFIT curve fits, residuals are plotted beneath the binding curves.) RAE1 mutants were injected at concentrations of 0.4, 0.8, 1.6, 3.2, and 6.5 μM. Wild-type RAE1γ, RAE1β, and RAE1δ were injected at five concentrations, 0.4, 0.8, 1.6, 3.2, and 6.5 μM, over the coupled m152 surface. RAE1ε was offered at concentrations of 1.6, 3.2, and 6.5 μM. (*C*) Values for K_d and k_{off} as determined in EVILFIT along with the rmsd of the global fits are tabulated.

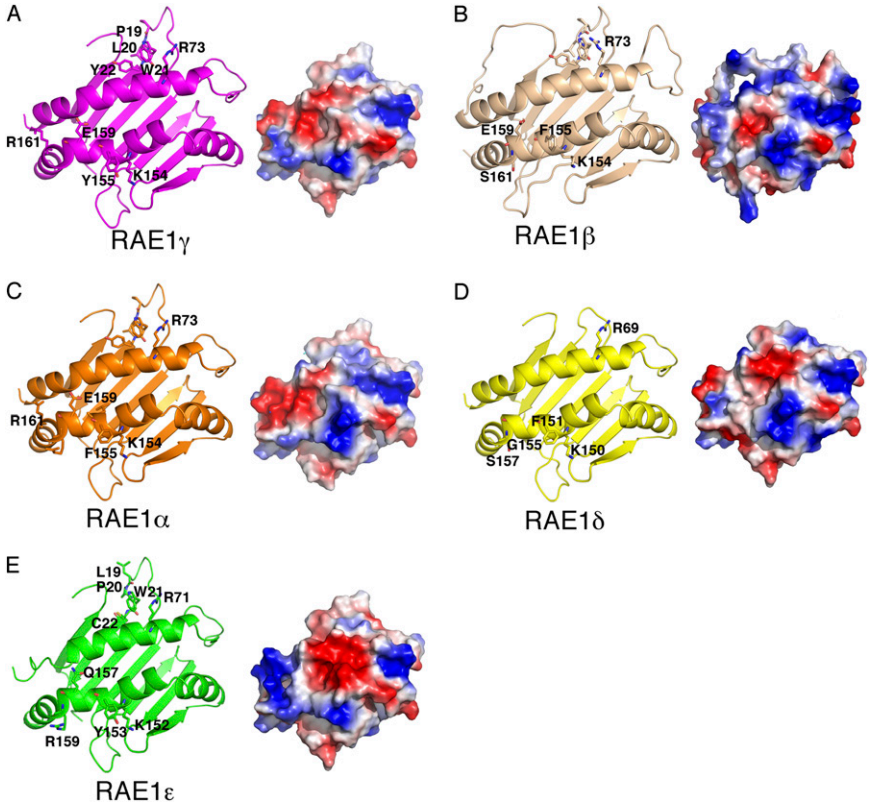

Fig. S4. Molecular models of RAE1 isoforms. Homology models of RAE1α (*C*), δ (*D*), and ε (*E*) were made based on the structure of RAE1γ (*A*) from the m152/RAE1γ complex using Coot (50). RAE1β (*B*) is chain A from RAE1β (PDB ID 1JFM). Ribbon diagrams and surface electrostatic representations were generated with PyMOL Molecular Graphics System, version 1.5.0.1 (Schrödinger, LLC, www.pymol.org).

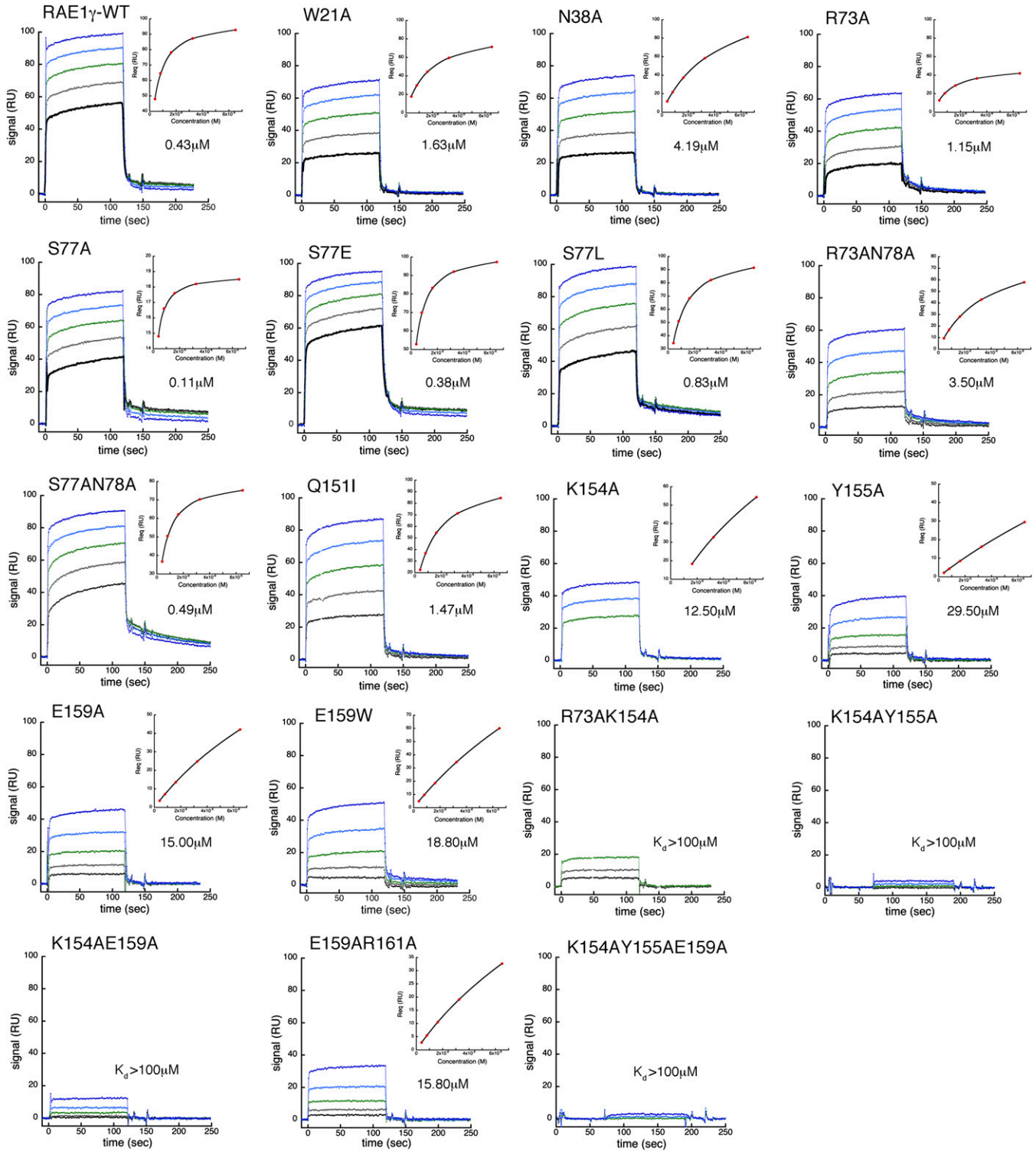

Fig. S5. SPR binding of wild-type RAE1γ and mutants to the NKG2D surface. mNKG2D-Fc was coupled to CM5 biosensor chips, and wild-type RAE1γ and RAE1γ mutants were injected sequentially. Calculated K_d values were determined by steady-state evaluation of global curve fits using BIAevaluation 3.0. *Insets* show plots of binding isotherms. Wild-type RAE1γ and most RAE1γ mutants were injected at five concentrations: 0.4, 0.8, 1.6, 3.2, and 6.5 μM. K154A, R73A/K154A, and K154A/Y155A/E159A mutants were injected at graded concentrations of 1.6, 3.2, and 6.5 μM.

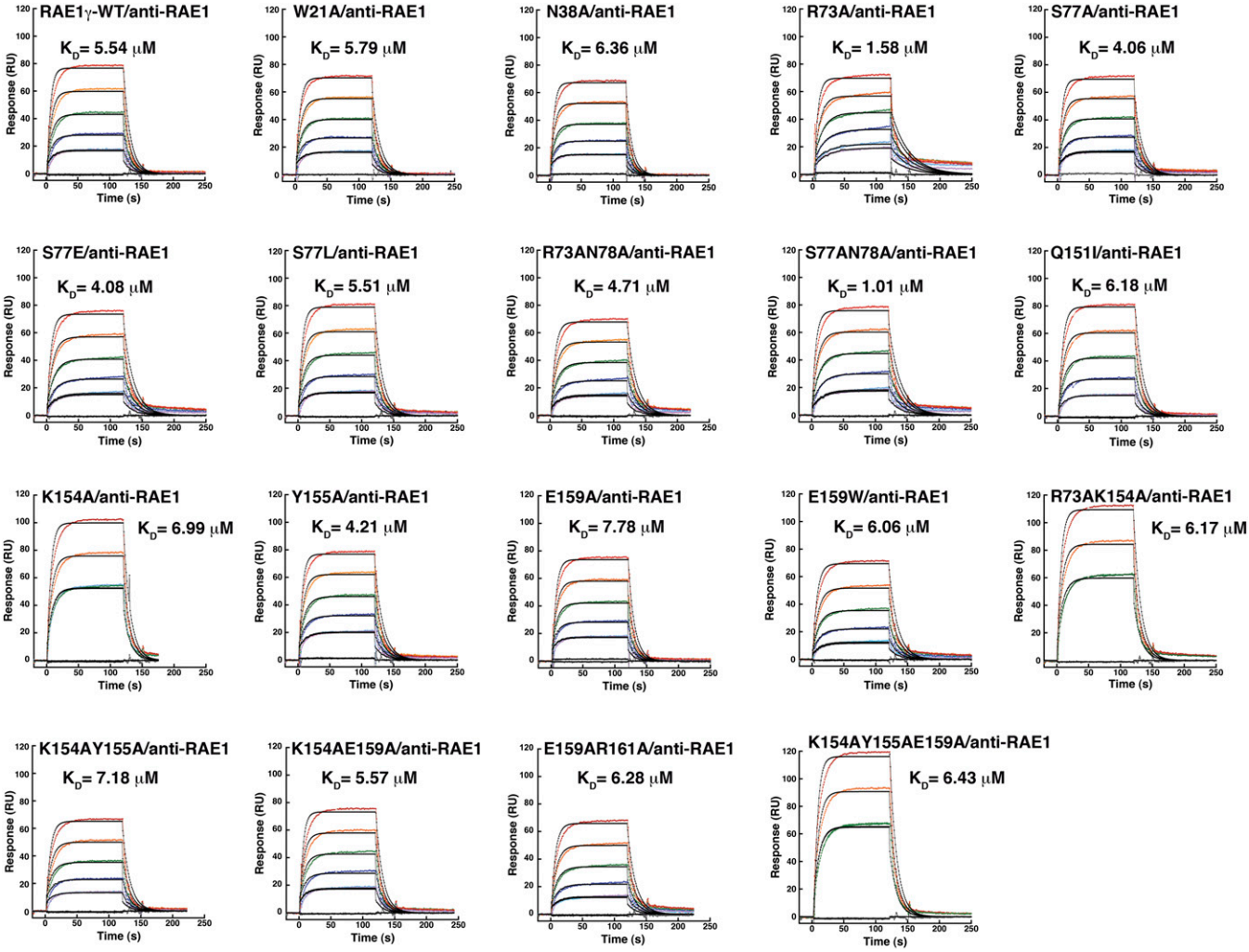

Fig. S6. SPR binding of wild-type RAE1γ and RAE1γ mutants to an anti-RAE1 surface. Anti-RAE1 antibody was coupled to CM5 biosensor chips, and wild-type RAE1γ or RAE1γ mutants were injected sequentially over the surface. The zero time point corresponds to the start of the injection, and buffer washout initiated the dissociation phase of the curves. Background binding to a mock-coupled surface was subtracted. Calculated K_d values were determined by global curve fits of the kinetics curves using BIAevaluation 3.0, because the high dissociation rate constant, makes these data unsuitable for EVILFIT. Wild-type RAE1γ and most RAE1γ mutants were injected at five concentrations: 0.4, 0.8, 1.6, 3.2, and 6.5 μM. K154A, R73A/K154A, and K154A/Y155A/E159A mutants were injected at graded concentrations of 1.6, 3.2, and 6.5 μM.

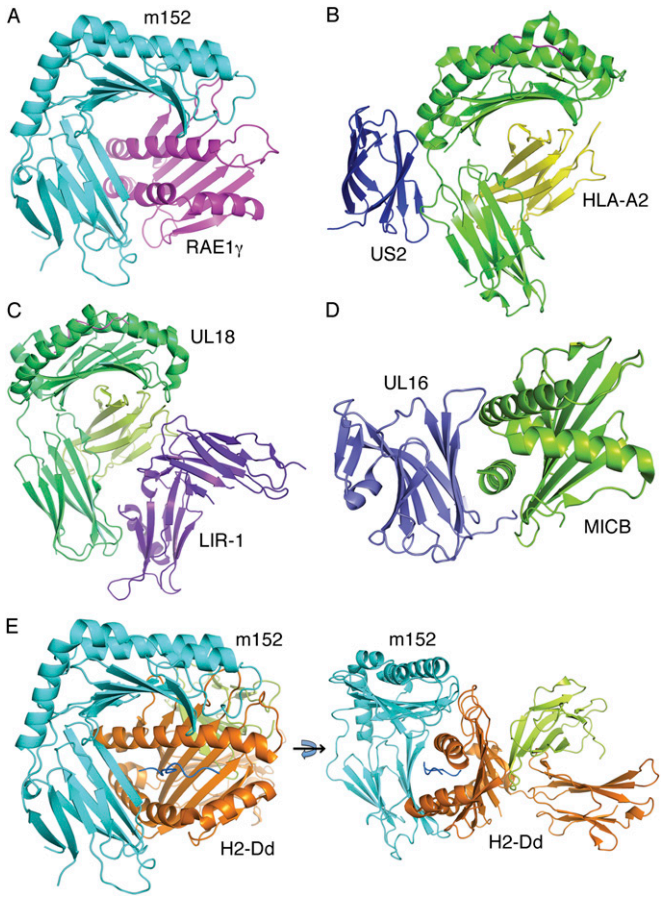

Fig. S7. Structural comparison of the m152/RAE1 complex with other cytomegalovirus (CMV)/host complexes. (*A*) Structure of m152 with RAE1γ. Colors are as in Fig. 1. (*B*) Structure of human CMX (hCMV) encoded US2 with HLA-A2 (PDB ID 1IM3). US2 is shown in blue, HLA-A2 heavy chain in green, β2m in yellow, and peptide in pink. (*C*) Structure of UL18 with LIR-1 (PDB ID 3D2U). UL18 heavy chain is shown in lime green, peptide in violet, and LIR-1 in purple/blue. (*D*) Structure of UL16 with MICB (PDB ID 2WY3). UL16 is shown in slate and MICB in chartreuse. All structures are shown as ribbon illustrations in the same orientation. (*E*) Structural model of m152 with H2-D^d complex. m152 is shown in cyan, H2-D^d heavy chain in orange, β2m in lemon, and peptide in marine. The H2-D^d model was derived from PDB ID 3ECB, and the m152 model was derived from the 152/RAE1γ structure.

Table S1. Data collection and refinement statistics for m152/RAE1γ

Data collection	
Space group	C2
Cell dimensions	
a, *b*, *c* (Å)	193.443, 99.800, 68.609
α, β, γ (°)	90.00, 100.72, 90.00
Resolution (Å)	50–2.45 (2.54–2.45)*
R_{sym} or R_{merge}	0.077 (0.578)
$I/\sigma I$	25.9 (2.8)
Completeness (%)	98.3(96.4)
Redundancy	7.5 (6.6)
Refinement	
Resolution (Å)	
No. reflections	45,215
R_{work}/R_{free}	0.20/0.24
No. atoms	
Protein	69,18
Carbohydrate	4
Water	75
B-factors	51.8
Protein	51.7
Carbohydrate	51.0
Water	48.2
Rmsd	
Bond lengths (Å)	0.009
Bond angles (°)	1.30
Ramachandran statistics	
Favored (%)	96
Outliers (%)	0.12

The dataset was collected on a single crystal.
*Values in parentheses are for highest-resolution shell.

Table S2. Interactions between m152 and RAE1γ

Hydrogen bonds (heterodimer 1. A, C chain)			Hydrogen bonds (heterodimer 2. B, D chain)		
RAE1γ	m152	Length (Å)	RAE1γ	m152	Length (Å)
Trp^{21} NE1	Glu^{28} O	2.8	Trp^{21} NE1	Glu^{28} O	2.9
Tyr^{22} OH	Glu^{28} OE2	2.7	Arg^{73} NE	Asp^{113} OD1	2.8
Arg^{73} NE	Asp^{113} OD1	2.9	Arg^{73} NH2	Tyr^{134} OH	3.0
Ser^{77} OG	Asp^{113} OD2	2.9	Lys^{154} NZ	Asp^{236} OD2	2.6
Asn^{78} OD1	Asn^{115} ND2	3.2	Glu^{159} OE1	Arg^{222} NH2	2.8
Lys^{154} NZ	Asp^{236} OD2	2.7	Glu^{159} OE2	Arg^{222} NE	2.9
Glu^{159} OE1	Arg^{222} NH2	3.0			
Glu^{159} OE2	Arg^{222} NE	2.9			

Table S3. Contacts between m152 and RAE1γ

	Contacts between m152 and RAE1γ (heterodimer 1. A, C chain) (distances <4 Å)		Contacts between m152 and RAE1γ (heterodimer 2. B, D chain) (distances <4 Å)	
	RAE1γ	m152	RAE1γ	m152
Binding site A	Pro^{14}	Ala^{89}, Gly^{90}	Ala^{13}	Tyr^{134}
	Pro^{16}	Lys^{88}	Pro^{14}	Ala^{89}, Tyr^{134}
	Pro^{19}	Pro^{30}	Pro^{16}	Lys^{88}
	Trp^{21}	Tyr^{26}, Glu^{28}, Gly^{90}, Pro^{92}	Pro^{19}	Pro^{30}
	Tyr^{22}	Glu^{28}	Trp^{21}	Tyr^{26}, Glu^{28}, Pro^{92}
	Asn^{38}	Glu^{28}, Gly^{29}, Met^{32}	Tyr^{22}	Glu^{28}
	Ile^{39}	Met^{32}	Ser^{37}	Glu^{28}
	Asn^{40}	Met^{32}	Asn^{38}	Glu^{28}, Glu^{29}, Met^{32}
	Lys^{41}	Met^{32}	Ile^{39}	Pro^{30}, Met^{32}
	Gln^{63}	Arg^{222}	Asn^{40}	Pro^{30}, Met^{32}
	Arg^{73}	Arg^{91}, Pro^{92}, Asp^{113}	Gln^{63}	Arg^{222}
	Asp^{74}	Asp^{113}, Gly^{114}	Asp^{67}	Arg^{222}
	Ser^{77}	Asp^{113}, Pro^{133}, Tyr^{134}	Arg^{73}	Pro^{92}, Asp^{113}, Tyr^{134}
	Asn^{78}	Asp^{113}, Asn^{115}, Pro^{133}	Asp^{74}	Asp^{113}
	Tyr^{89}	Tyr^{134}	Ser^{77}	Asp^{113}, Pro^{133}
	Pro^{90}	Tyr^{134}	Asn^{78}	Asp^{113}, Asn^{115}, Pro^{133}
			Gly^{88}	Tyr^{134}
			Tyr^{89}	Tyr^{134}
Binding site B	Thr^{105}	Gly^{191}	Met^{127}	Arg^{238}
	Met^{127}	Arg^{238}	Gln^{151}	Tyr^{218}
	Gln^{151}	Tyr^{218}	Arg^{152}	Tyr^{218}
	Arg^{152}	Tyr^{218}	Lys^{154}	Tyr^{194}, Asp^{236}
	Lys^{154}	Tyr^{194}, Asp^{236}	Tyr^{155}	Tyr^{218}, Asp^{236}, Trp^{234}
	Tyr^{155}	Tyr^{194}, Tyr^{218}, Trp^{234}, Asp^{236}	Pro^{158}	Trp^{234}
	Pro^{158}	Trp^{234}	Glu^{159}	Tyr^{220}, Arg^{222}, Glu^{232}, Trp^{234}
	Glu^{159}	Tyr^{220}, Arg^{222}, Glu^{232}, Trp^{234}	Arg^{161}	Asn^{189}, Asn^{192}
	Arg^{161}	Tyr^{187}, Asn^{189}		

Table S4. Comparison of amino acid contacts at the m152/RAE1γ and mNKG2D/RAE1β interfaces

				Murine NKG2D	
	RAE1γ	m152	RAE1β	A chain	B chain
Binding site **A**	Pro14	Ala89, Gly90	Pro14	Ile200	
	Pro16	Lys88	Pro16	Lys202	
	Pro19	Pro30			
	Trp21	Tyr26, Glu28, Glu90, Pro92	Trp21	Tyr168	
	Tyr22	Glu28			
	Asn38	Glu28, Gly29, Met32			
	Ile39	Met32			
	Asn40	Met32			
	Lys41	Met32			
	Gln63	Arg222			
			Gln70	Ser167, Tyr168	
	Arg73	Arg91, Pro92, Asp113	Arg73	Tyr168, Tyr215	
	Asp74	Asp113, Gly114	Asn74	Tyr215	
	Ser77	Asp113, Pro133, Tyr134			
	Asn78	Asp113, Asn115, Pro133			
	Tyr89	Tyr134			
	Pro90	Tyr134			
	Thr105	Gly191			
Binding site **B**	Met127	Arg238			
			Glu148		Lys166, Ser167
	Gln151	Tyr218	Lys151		Tyr168, Glu217, Asn223
	Arg152	Tyr218			
	Lys154	Tyr194, Asp236			
	Tyr155	Tyr194, Tyr218, Trp234, Asp236	Phe155		Tyr168, Tyr215
	Pro158	Trp234	His158		Ile200
	Glu159	Tyr220, Arg222, Glu232, Trp234	Glu159		Lys213, Tyr215
	Arg161	Tyr187, Asn189			